Soft and Steady Wins the Race

Model-based design for an adaptive soft meta-mechanism for locomotion on deformable terrain

Pans, Gaetan; Chen, Qianyi; Jovanova, Jovana

DOI
10.1109/RoboSoft63089.2025.11020863

Publication date
2025

Document Version
Final published version

Published in
Proceedings of the IEEE 8th International Conference on Soft Robotics, RoboSoft 2025

Soft and Steady Wins the Race: Model-based design for an adaptive soft meta-mechanism for locomotion on deformable terrain

Gaetan Pans[1], Qianyi Chen[2*] and Jovana Jovanova[3]

2025 IEEE 8th International Conference on Soft Robotics (RoboSoft) | 979-8-3315-2020-5/25/$31.00 ©2025 IEEE | DOI: 10.1109/RoboSoft63089.2025.11020863

***Abstract*— The importance of natural environments with rugged deformable terrain from biodiversity, carbon capture, and coastal protection to economic livelihood is significant. However, the current systems available for robots to explore those ecosystems are either large, expensive and intrusive, not application focused or consist of many mechanical parts prone to failure. This study proposes a soft adaptable wheel designed and verified using a novel modelling-based approach suited for such ecosystems. The novel modelling techniques used a 3 part iterative design framework including a kinematic analysis using multi-body dynamics, structural feasibility tests using the finite element method and deformable terrain testing using the discrete element method. The final design operates as a soft fluidic actuator constructed with silicone, able to change its form depending on the task at hand. The proposed model is intended to be a more application-driven design (for rugged deformable terrain), that can more easily be integrated into robotic systems using off-the-shelf components. The simplicity and symmetry of the model can be easily scaled according to the terrain type, load requirements or application of the robotic system, ultimately reducing the time required to be used in environmental applications.**

Keywords

Soft Robotics, Deformable Terrain, Soft Fluidic Actuator, Modelling, Locomotion

I. INTRODUCTION

The world has an abundance of natural environments that consist of rugged outdoor obstacles that have deformable terrain. Deformable terrains refer to areas with granular material that yields almost instantly under pressure, with little recovery in shape and its rheological properties are highly affected by moisture [29]. This makes it inherently difficult for robotic systems to effectively move through these areas that are constantly shifting. However, due to the economic and environmental importance of these environments, it is crucial to have robots that can effectively traverse these areas, in a non-intrusive, non-toxic and effective manner. Current commercial systems, like off-road vehicles, are large, expensive, and damaging to the environment. While smaller multi-terrain robots, such as SeaDog by Klein et al. [27], have been proposed, they are still rigid (causing damage to the surrounding environment) and lack the adaptability needed to overcome varying deformable terrain. Though biomimetic soft designs have made strides, such as an eelworm-inspired robot with soft fluidic actuators [22], snake-like robots using McKibben actuators [23], frog-inspired jumping robots [24], and turtle-inspired designs with shape memory alloy wires embedded in polymer composites [26], they often remain tethered to labs due to high power requirements and complexity, limiting practical industrial application [21]. Tolley et al.'s multi-modal robot [25] is a notable exception, though the velocity is relatively slow, and its unique design is difficult to incorporate into traditional robotic systems. This study proposes a solution that balances the flexibility of soft actuators, which mimic materials found in nature with elastic moduli in the range of 10^4 to 10^9 Pa [28], with the practicality of traditional robotic components. To model such a system, multiple approaches have been explored. Wang et al. created SoftZoo focusing on co-optimisation between morphology and control of a robot in diverse environments [30]. Although efficient in its modelling of deformable terrain, the tool designed did not include any obstacles for the robot to overcome or analysis of the material limitations of soft actuators to generate those movements. Traditional methods also involve the finite element method which is commonly used for a specific soft component of the whole system due to its ability to capture non-linear behaviour [32]. Although this has become common in many commercial pieces of software however it is usually used as an independent design step not informed by other modelling approaches. Hence, a more informed decision can be made by coupling various modelling techniques to ensure as many components of the robotic design process are covered.

II. DESIGN METHODOLOGY

With the desired terrain and problem outlined, the specific design requirements set for the robotic system are as follows:

- Able to locomote over deformable terrain of varying moisture levels.
- Able to withstand a load of 1.25N (to operate on a 500g robot, assuming 4 wheels).
- Non-destructive or intrusive to the surrounding environment.
- Non-toxic to the surrounding environment.

The design methodology proposed in this study captures the 3 key components of the problem using an iterative design approach as seen in Figure 1. This includes the robot kinematics, the structural feasibility of the soft mechanism under loading and finally its interaction in deformable terrain. The robot kinematics was achieved using multi-body dynamics (specifically MuJoCo) to test how different design parameters (number of paddles and shape of paddles) affect its ability to overcome varying obstacles. The scientific conclusions from this point were used to make informed

[1]Gaetan Pans is with the Faculty of Mechanical Engineering, Delft, University of Technology, 2628CD Delft, The Netherlands; email: gpans@tudelft.nl

[2*]Qianyi Chen is with the Faculty of Mechanical Engineering, University of Technology, 2628CD Delft, The Netherlands corresponding author to provide phone: +310613989827; e-mail: Q.Chen- 5@tudelft.nl

[3]Jovana Jovanova with the Faculty of Mechanical Engineering, University of Technology, 2628CD Delft, The Netherlands; email: J.Jovanova@tudelft.nl

decisions towards an initial soft robotic design. This design was then modelled and improved upon to ensure it could meet the loading requirements given its material properties using the finite element method. Once a final adaptive soft design was obtained, it was tested in its key operating configurations in varying deformable terrains using the discrete element method coupled with another multi-body dynamics software.

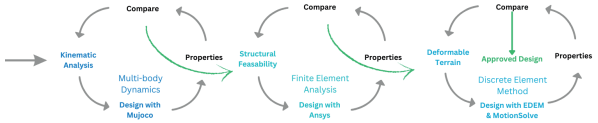

Fig. 1. Design methodology

The use of this modelling approach means that all important elements that affect the success of the design could be tested and fed into the next design loop. Hence, despite limitations in available modelling software to fully capture the problem in one program, coupling various techniques allows an informed decision to be made about the entire design problem without having to make a physical prototype. The starting design for this project was a cyclic paddler, which is a component that has a central rotation element with radially expanding paddles to help it overcome obstacles (seen in Figure 2). The use of a cyclic paddler (combining the kinematic benefits from rolling and paddling as per a study done by Shui et al.[1]) has proven to be successful in overcoming obstacles whilst easily integrating with standard robotic components. This study aims to bridge the gap by proposing a design that leverages the benefits of soft actuators known for their high strain tolerance and flexible nature—while maintaining the practical, application-focused mindset of traditional robotics with the starting point for the design being a cyclic paddler.

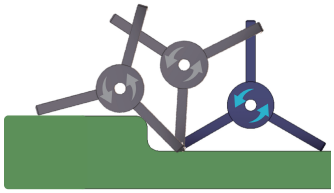

Fig. 2. Starting design of a cyclic paddler

III. MODELLING TECHNIQUES

A. Kinematic analysis through a multi-body dynamics study

Setup

The initial design cycle was focused on evaluating how the number and shape of paddles influence a robot's ability to overcome various obstacles. This evaluation was carried out using the MuJoCo robotic simulator in Python. A total of 8 different paddle configurations were tested—ranging from 1 to 4 paddles and from straight to curved shapes—alongside a standard wheel used as a control. These variations, as shown in Figure 3, were assessed under identical conditions, with the wheel radius kept constant, ensuring that only the paddle quantity and shape affected performance.

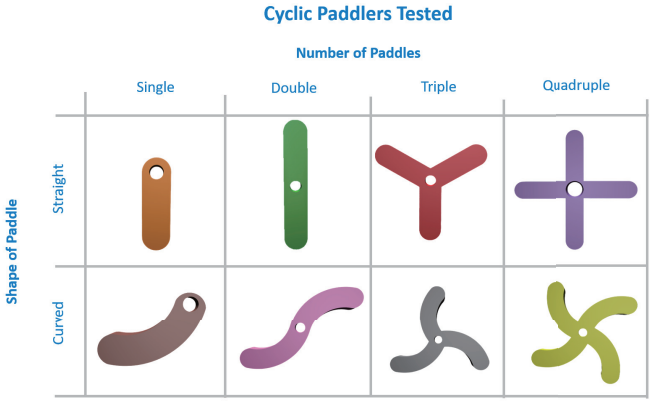

Fig. 3. Range of cyclic paddles tested

To test the cyclic paddles, a base robot with 4 axles was used, to which the various cyclic paddlers could be attached. The 4 cyclic paddlers that are connected through the hinge joint are structured in the XML file as a child of the robot body. Each joint is then given an increasing rotational velocity (over 1 second, levelling off at 2π rad/s using a proportional differential controller), a damping coefficient of 0.2 to ensure stable rotation and simulated for a total of 10.5 seconds in various terrains. To simulate the terrain, greyscale generation was used alongside Perlin Noise for the more complex topographies. To generate the terrains, greyscale images were created in Python to represent the topography. Black pixels indicate the lowest points, white pixels the highest, with a linear gradient for everything in between. This is then extrapolated into a 3D surface mesh by using the height field function in MuJoCo providing the X, Y, and Z extremities of the terrain, of which an example can be seen in Figure 4. For each terrain, the robot is able to move through an 2500m^2 area (50 x 50m) with the height being a function of the type of terrain and experiments to be conducted. For the more complex terrains (undulating smooth and terraced of Figure 5), Perlin noise generates a noisy greyscale image before being converted into a 3D mesh using the height field function.

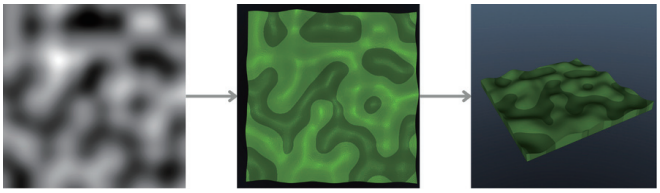

Fig. 4. Greyscale terrain generation

The terrains simulated were flat, steps, ramp, undulating and terraced according to the design requirements and can be seen in Figure 5.

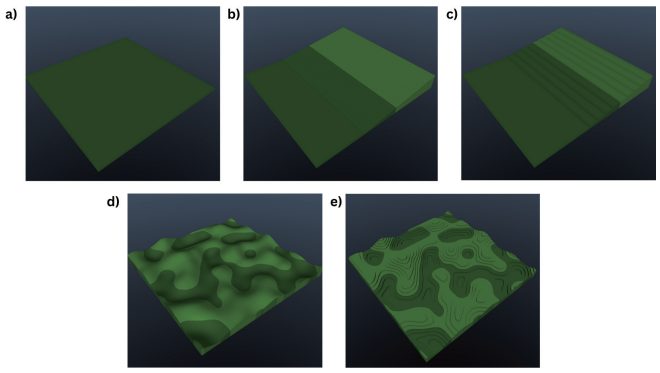

Fig. 5. Terrain Types: a) flat b) steps c) ramp d) undulating (smooth) e) undulating (terraced)

The final addition to the model is to set the friction coefficients between the robot and the terrain. The friction is set as a property of the robot geometry, defining the coefficients of friction as well as the dimensionality of the contact space in which the model checks for contact between two geometries. The dimensionality (set using the condim variable) was set to 3 applying regular frictional contact and opposing slip in the tangent plane. The default time step was used 0.002s, as this favours stability and accuracy over the model's efficiency. For the coefficients of friction, values from a tyre sand interaction from the literature were used as an approximation [31]. This is because the actuation method is known to be soft, meaning the material will be rubber/silicone-based and the terrain intended is deformable. From this, the sliding friction, torsional friction and rolling friction were set as 0.6, 0.005 and 0.2 respectively. For all terrains, the robot was placed in front of the main obstacle (e.g. the slope) beside terrains d and e from Figure 5. The location in which the robot is placed may affect its performance due to the random nature of the terrain. Due to this, for those 2 terrains only, the robot will be randomly dropped 3 times and the results averaged accordingly. The total number of simulations to be run was 81 accounting for the 9-wheel designs, all terrains, and the repeats on the smooth and terraced terrain. The metric for comparison was the distance travelled based on a sensor added to the centre of the robotic body that records its Cartesian coordinates during the simulation.

Results

With all 81 experiments run, both quantitative (from the data) and qualitative aspects (from analysing the simulation videos) were used to inform the decision of the final geometry. The first main conclusion is that the designs that had multiple limbs (triple and above) performed better than those with single or double limbs. With triple and quadruple designs, all travelling above 8m on all terrains and single designs travelling less than 5m across all terrains, it is clear that a higher number of limbs is beneficial. The second key conclusion is they curved legs performed better on flat and ramped terrains, whereas straight legs are more suitable for the remaining terrains. Designs with a higher number of limbs were more stable, maintained a higher speed due to increased contact with the ground, and were able to better overcome the complex topographies of the undulating terrains. The structure in the designs of 3 limbs and more meant that no matter how it landed, there was always a component in contact with the terrain. In other single and double-legged designs, problems such as 1 limb facing a completely different direction from the other 3 due to the terrain, resulting in requiring a much larger torque to overcome its weight and generate locomotive motion, were very common. In general, it was seen that its ability to upright itself, when knocked over, is more important than being able to move quickly across a terrain. This would be even more important in the real world, as disturbances such as animals or weather would be present. Hence, the following 4 design conclusions were obtained from the first design cycle. A high number of paddles is favourable, an adaptable height and contact area is desirable, and finally, the ability to individually actuate each paddle is highly beneficial for complex topographies. The proposed design following these conclusions is a completely soft wheel with 4 limbs, where each limb is made up of inflatable hollow chambers similar to those in traditional soft grippers. The individual limb design is based on a common soft fluidic actuator which couples the inflatable hollow chambers with a strain-limiting layer on one side. When pressurised in a spatio-temporal manner, the stiffness differential causes deliberate and controlled deformation in one direction. Common shape configurations include pleated (also known as Pneunet), ribbed and cylindrical. As studied by Marchese et al., the pleated structure generates the highest tip force of the 3 configurations [3]. The wheel's controlled deformation adjusts its curvature and height, allowing the robot to adapt to rugged terrain, which also enables the robot to climb over obstacles with extended limbs, pass under tight spaces by deflating them, and increase ground contact to prevent sinking in soft terrain. As shown in Figure 6, the neutral position is placed at maximum curvature such that at 0 pressure, the structure is still stable and cannot deform past the geometrical limit. The chambers are trapezoidal to make use of the stability of a triangular surface. The neutral configuration has a height of 230mm, with the fully inflated wheel having a height of 280mm.

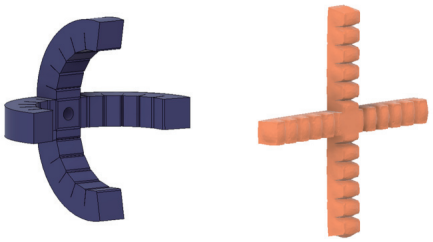

(a) Neutral Wheel (b) Inflated Wheel

Fig. 6. Proposed design

B. Numerical and analytical model of soft wheel

Setup

With the proposed design only being simulated up to this point as a rigid body, it needed to be ensured that it is structurally feasible if made out of a soft material. For this first, the system needs to be characterised by understanding the required inflation pressure to actuate the system from natural to fully inflated (i.e. a pressure with bending angle

relationship). Once this was understood, the system could be modelled with the required external loads. For the simulation, a static structural analysis of the hyperelastic material used was run using FEM by commercial software (the numerical model). To improve computational efficiency, the model was simplified to a single limb, focusing on the point of contact with the ground, which bears the highest loads. Simulating only a quarter of the design reduced the number of mesh elements and computation time. Silicone-based polymers are the primary choice for soft actuators due to their high maximum strain value [7] and being non-toxic to the surrounding environment. Hence, the elastomer with the highest shore hardness of the Dragon Skin series whilst maintaining a high strain failure rate [18] was selected. Various strain energy functions (Ψ) can be used to characterise the hyperelastic model. For Dragon Skin 30, the 2nd-order incompressible Yeoh Model was most suitable to capture the stress-strain response, as it's suitable for large strain problems at or above 400% [5]. The experimental values obtained from Yang et al. for loading under uniaxial tension are $C_1 = 114.88$ kPa and $C_2 = 1.262$ kPa [17].

$$\Psi = C_1(I_1 - 3) + C_2(I_1 - 3)^2 \tag{1}$$

As for the simulation setup, a mesh size of 3mm was selected alongside linear order elements [5]. This facilitated convergence (using a coarse mesh size) whilst capturing the large deformation of each chamber, as found by Tawk and Alici [4]. A frictional contact was set between all outer walls between the chambers with a coefficient of 0.2. To verify the FEM model, an analytical model was developed. The analytical model is based on the principle of minimum potential energy (Γ) applied to an individual soft chamber. This can be defined as the sum of the internal material strain energy (U) and the work potential (W_p), This model builds on the approach proposed by Cao et al. [2]. As work is being done on the system (in this case pressure), it is assumed that the deformation caused is perfectly elliptical, resulting in an overall uniform curvature of the actuator as seen in Figure 7.

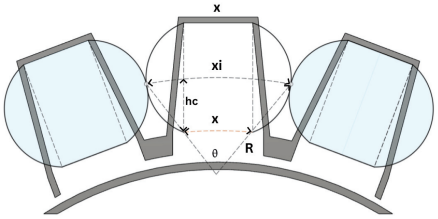

Fig. 7. Schematic and geometry of the inflated chambers

From this, the following geometrical relationships can be made:

$$\theta = \frac{x_i}{R} = \frac{x}{R - h_c} \tag{2}$$

$$V_i = \frac{\pi}{4} h x_i d_c \tag{3}$$

Where the subscript i refers to the property when inflated. θ is the bending angle, R is the radius of curvature, x is the original chamber width, and x_i is the maximum inflated chamber width found at the centre of the ellipse. Additionally, h_c represents the distance to the centreline of the ellipse, h_1 is the distance from the base of a chamber to the top of the strain-limiting layer, and h is the total height of a chamber. d represents the depth of the entire actuator, where d_c represents the depth of just the internal chamber. Lastly, V_i denotes the inflated volume of a chamber.

(Γ) can be expressed as the internal strain energy of one chamber minus the work done due to the applied pressure to that chamber.

$$\Gamma = \frac{1}{2} D k_i^2 x_i - P_i V_i \tag{4}$$

where k is the curvature, D is the flexural rigidity, E is the elastic modulus, and I is the moment of inertia of the chamber ($\frac{dh_1^3}{12}$). Additionally, P_i represents the inflation pressure. However, due to the hyperelastic material properties, the elastic modulus cannot be constant and instead is a function of the strain. Using the Yeoh hyperelastic model, the uniaxial stress-strain relationship can be obtained (adopted from [5]). From here, the gradient can then be used as a function of strain to accommodate for the non-linearity. The point of equilibrium can then be found by solving $\frac{\partial \Gamma}{\partial k} = 0$. Solving for k and simplifying (taking the minimum of the quadratic solutions), followed by combining the simplified expression alongside Equation (2), the equation for the bending of one chamber can be obtained. With the assumption that bending is uniform, the final expression for the bending curvature of the entire structure as a function of pressure is as follows, where N is the number of chambers:

$$N\theta = \frac{Nx\left(EI - \sqrt{(EI)^2 - \frac{1}{2}\pi EI d_c h h_c^2 P_i}\right)}{h_c \sqrt{(EI)^2 - \frac{1}{2}\pi EI d_c h h_c^2 P_i}} \tag{5}$$

This analytical model is used to verify the bending angle against pressure relationship from simulations before simulating the remaining loading configurations. The bending angle in the simulation is determined by adding a probe on the end face that captures the average Eulerian angle between the starting position of the face and the end position. For this characterisation, both the analytical model and numerical model were modelled with an inflation pressure of 0 - 30kPa. Once verified, the design is simulated using the numerical model in 2 key loading configurations. Firstly, a 0kPa pressure load test was conducted to ensure the design can support its self-weight even if not inflated. The self-weight as set by the requirements is a load of 1.25N. The second loading configuration is a blocked force test where the point of contact with the ground is fixed, and the pressure is ramped up from 0-50kPa. Through this, the maximum loading conditions of the design can be quantified to see the exerted force when changing the wheel's shape. For both of the loading configurations, acceleration due to gravity is also considered in the model. For the set of simulations, the maximum strain, maximum stress overall deformation profile are analysed to ensure no material failure as well as to understand operational characteristics. Material failure for Dragon Skin 30 occurs at a true stress value of 34MPa and strain of 700% [17].

Results

For verification of the model, it can be seen in Figure 8 that there is a strong agreement between the bending angle relationship derived from the 2 modelling methods, with a

mean absolute error of 2.51°. Alongside the verification, under maximum pressure (30kPa) with no external loading, it was seen that no material failure occurred and that the strain distribution was uniform. This is key in the design of soft actuators to ensure no blockages in the design of the chambers.

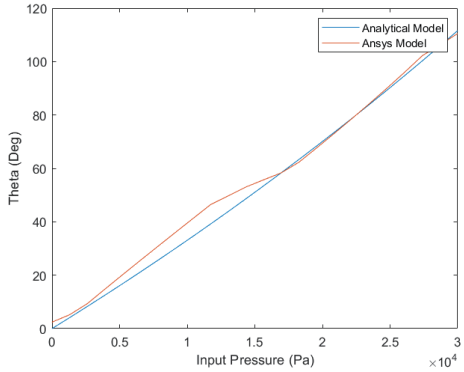

Fig. 8. Comparison of bending angle as a function of internal pressure for the final design, comparing the analytical and numerical results

It was seen that the final design proved stable at a 0kPa load test under 1.25N. The change in bending angle was negligible with the trapezoidal design acting as intended, to maintain the form of the wheel. This means that if needed, a robot (of 500g assuming 4 wheels) could maintain operational even if no power was available for the shape change. Regarding the blocked force test, peak pressures of 50kPa produced a value just upwards of 3N. However, when analysing the strain values at that point, despite no material failure, the distribution became significantly non-uniform and wouldn't provide stable operation. Hence, the operating blocked force was taken as 1.98N (at 35kPa) as that was the point where all chambers were still a uniform volume maintaining the curvature of the limb as seen in Figure Figure 9. The maximum stress and strain values were well below a point of material failure for all load cases. The characterisation model with zero external load and just pressure experienced a maximum stress of 449 kPa and strain of 0.69. The zero pressure load test resulted in maximum stress and strain values of 848 kPa and 0.37 respectively. Finally, the blocked force test had maximum stress and strain values at its operational point of 878 kPa and 1.23 respectively.

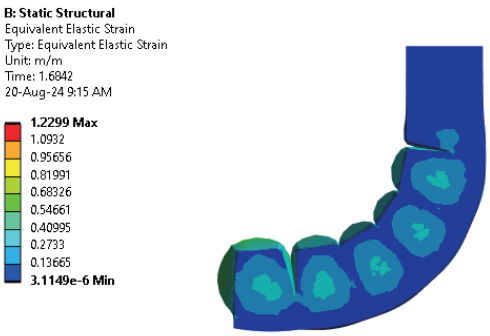

Fig. 9. Strain distribution at maximum operating pressure (35kPa)

C. Modelling of the deformable terrain and coupling Setup

Once the model has been tested structurally, the DEM modelling coupled with multi-body dynamics was used to test the resultant design in its desired deformable terrain. Terrains of varying moisture and compressibility are tested to determine the versatility of the design. In the modelling, the built-in terrain material database from commercial software [19] was used, which includes the following four particle types: non-compressible dry, compressible dry, non-compressible sticky, and compressible sticky. The robot-particle interaction properties were sourced from tyre and sandy soil studies [20]. The coefficient of restitution varied linearly between 0.48 and 0.36 from non-compressible dry, non-compressible sticky, compressible dry and compressible sticky respectively. In addition, the Dragon Skin 30 is simplified to the standard rubber parameter for coupling. The sliding friction and rolling friction are set to 0.55 and 0.37 respectively. Due to the high computation required in generating a large number of particles, the terrain is limited to a size of 3m x 4m x 0.8m. In addition, 3 key operating configurations were chosen and exported in their deformed state, including a neutral state, a fully inflated state (shown in Figure 6) and a wheel inflated to the halfway point (15kPa at no-loading). For each simulation, the terrain (30,000-35,000 particles) was filled and settled before coupling with the commercial software. The goal was to measure how far different wheel configurations travelled across various terrains in 5 seconds, with each joint set to a constant velocity of 2π rad/s. MotionSolve then dropped the robot into the terrain and applied the forward velocity as seen in Figure 10. This process was repeated for each wheel configuration, running 12 simulations (4 sand types, 3 wheel configurations).

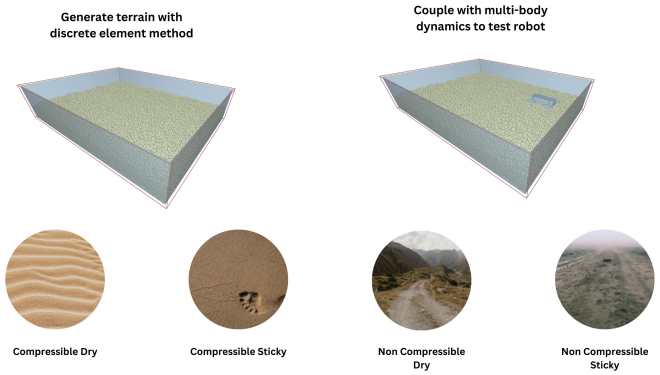

Fig. 10. Schematic for the simulation setup of the deformable terrain testing

Results

The results of concern are the distance travelled and the ride height (how much each design sinks into each terrain). From the data, it is seen that, on average, the neutral configuration has the highest ride height in comparison with the remaining two. With values of 72mm, 70mm and 55mm for neutral, fully inflated and partially inflated respectively. This is due to its larger plane of contact with

the ground, resulting in more support to minimise how much the structure sinks into the deformable terrain. Interestingly, the partially inflated is the lowest due to its partial inflation creating a line point of contact instead of a flat plane (as with the fully inflated) resulting in it digging itself into the ground. When looking at specific sand types, the need for various configurations for ride height becomes clear. Within compressible sticky and non-compressible dry, the neutral wheel has the highest ride height (74mm and 71mm respectively), whereas in the remaining 2 sand types a fully inflated wheel performs best (85mm and 66mm). When looking at the distance travelled across the terrain, the fully inflated wheel travels the furthest in all sand types (average of 3.4m). This is consistent with its diameter being physically larger than the other configurations, meaning every rotation physically travels a larger distance. However, despite being the smallest in diameter, the neutral configuration travels the second furthest (average of 2.9m). The low ride height of the partially inflated wheel results in it having to do more work to move through this terrain despite having a larger diameter, resulting in the lowest average distance of just 2.6m.

IV. DISCUSSION

The proposed adaptable soft wheel model was developed through an iterative design cycle using three modelling techniques. Multi-body dynamics indicated the need for a high number of paddles and adaptability to navigate obstacles. These findings informed the next design cycle, which moved into the soft domain. The design used a common pleated structure in soft fluidic actuators, with a neutral curved configuration that inflated to increase height and reduce contact area. Dragon Skin 30 was used for the structure, modelled with an analytical and numerical method. Once structural requirements were met, the model was tested in 4 sand types and 3 operating modes using the discrete element method. The fully inflated wheel travelled the farthest, but had a lower ride height than the neutral configuration. Transitioning between states proved inefficient, being the most submerged, which helps inform future control strategies. Adaptability was beneficial across terrains, with wheel geometry, contact area, and moisture levels impacting performance. The design's simplicity allows integration with traditional robotic components, as well as easy scalability according to terrain and application. Applications include agriculture, biodiversity monitoring, mangrove reforestation, and even space exploration, where the wheel can compress for transport and inflate "on-site." Future work includes prototyping, real-world testing, and developing control strategies specifically for individual paddle actuation for greater compliance. This proposed design is aimed to be a starting point to increase the reach of robotic systems in environmental applications in a non-hazardous or damaging matter (with an example seen in Figure 11).

V. CONCLUSION

The iterative design approach was essential in refining the proposed mechanism. Coupling various models made the design more informed and application-specific. The design supports a 1.25N load in compression (at 0kPa) and a maximum blocked force of 1.98N at 35kPa. It was tested in various terrain types to validate its adaptability. The pneumatic wheel changes height between 230-280mm, offering scalable use for environmental exploration.

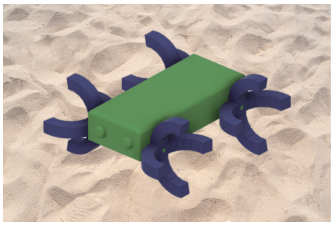

Fig. 11. Example schematic of full scale robot in deformable terrain

VI. ACKNOWLEDGMENT

This work is financially supported by Delft University of Technology. In addition, thanks for the support from the IWS 3D printing workshop and experiments lab in the Faculty of Mechanical Engineering, Delft University of Technology.

REFERENCES

[1] Shui, L., Zhu, L., Yang, Z., Liu, Y. & Chen, X. Energy efficiency of mobile soft robots. *Soft Matter*, **13**, 8223-8233 (2017).

[2] Cao, G., Chu, B. & Liu, Y. Analytical modeling and control of soft fast pneumatic networks actuators. In *Proceedings of the 46th Annual Conference of the IEEE Industrial Electronics Society (IECON)*, 2760-2765 (2020).

[3] Marchese, A., Katzschmann, R. & Rus, D. A recipe for soft fluidic elastomer robots. *Soft Robotics*. **2**, 7-25 (2015)

[4] Tawk, C. & Alici, G. Finite element modeling in the design process of 3D printed pneumatic soft actuators and sensors. *Robotics*. **9**, 52 (2020)

[5] Xavier, M., Fleming, A. & Yong, Y. Finite element modeling of soft fluidic actuators: Overview and recent developments. *Advanced Intelligent Systems*. **3**, 2000187 (2021)

[6] Smooth-On, I. Dragon Skin 30 Product Information. (2024), https://www.smooth-on.com/products/dragon-skin-30/, Accessed: 2024-07-29

[7] Trivedi, D., Rahn, C., Kier, W. & Walker, I. Soft robotics: Biological inspiration, state of the art, and future research. *Applied Bionics And Biomechanics*. **5**, 99-117 (2008)

[8] Ching, T., Lee, J., Win, S., Win, L., Sufiyan, D., Lim, C., Nagaraju, N., Toh, Y., Foong, S. & Hashimoto, M. Crawling, climbing, perching, and flying by FiBa soft robots. *Science Robotics*. **9**, eadk4533 (2024)

[9] Patel, A. Design and Analysis of Soft Actuator with Enhanced Stiffness with Granular Jamming. (University of Windsor (Canada),2022)

[10] El-Atab, N., Mishra, R., Al-Modaf, F., Joharji, L., Alsharif, A., Alamoudi, H., Diaz, M., Qaiser, N. & Hussain, M. Soft actuators for soft robotic applications: A review. *Advanced Intelligent Systems*. **2**, 2000128 (2020)

[11] Yap, Y., Sing, S. & Yeong, W. A review of 3D printing processes and materials for soft robotics. *Rapid Prototyping Journal*. **26**, 1345-1361 (2020)

[12] Shepherd, R., Ilievski, F., Choi, W., Morin, S., Stokes, A., Mazzeo, A., Chen, X., Wang, M. & Whitesides, G. Multigait soft robot. *Proceedings Of The National Academy Of Sciences*. **108**, 20400-20403 (2011)

[13] Tolley, M., Shepherd, R., Mosadegh, B., Galloway, K., Wehner, M., Karpelson, M., Wood, R. & Whitesides, G. A resilient, untethered soft robot. *Soft Robotics*. **1**, 213-223 (2014)

[14] Du Toit, V. Characterising material models for silicone-rubber using an inverse finite element model updating method. (Stellenbosch: Stellenbosch University,2018)

[15] Porte, E., Eristoff, S., Agrawala, A. & Kramer-Bottiglio, R. Characterization of temperature and humidity dependence in soft elastomer behavior. *Soft Robotics*. **11**, 118-130 (2024)

[16] Ghamsari, Z. The Introduction and Analysis of a Novel Soft Actuator for a Soft Continuum Robot Arm. (University of Minnesota,2018)

[17] Yang, F., Ruan, Q., Man, Y., Xie, Z., Yue, H., Li, B. & Liu, R. Design and optimize of a novel segmented soft pneumatic actuator. *IEEE Access*. **8** pp. 122304-122313 (2020)

[18] Agarwal, G., Besuchet, N., Audergon, B. & Paik, J. Stretchable materials for robust soft actuators towards assistive wearable devices. *Scientific Reports*. **6**, 34224 (2016)

[19] Altair Engineering Inc. (2022). *Soils Starter Pack*. Available at: `https://2022.help.altair.com/2022.2/EDEM/Creator/Soils_Starter_Pack.htm` [Accessed: August 11, 2024].

[20] Hu, C., Gao, J., Diao, J. & Song, X. Numerical simulation of tire steering on sandy soil based on discrete element method. *AIP Advances*. **11** (2021)

[21] Bai, X., Shang, J., Luo, Z., Jiang, T. & Yin, Q. Development of amphibious biomimetic robots. *Journal Of Zhejiang University-SCIENCE A 2022 23:3*. **23**, 157-187 (2022,3), https://link-springer-com.tudelft.idm.oclc.org/article/10.1631/jzus.A2100137

[22] Milana, E., Raemdonck, B., Cornelis, K., Dehaerne, E., Clerck, J., Groof, Y., Vil, T., Gorissen, B. & Reynaerts, D. EELWORM: A bioinspired multimodal amphibious soft robot. *2020 3rd IEEE International Conference On Soft Robotics, RoboSoft 2020*. (2020)

[23] Fracczak, Ł., Olejniczak, M. & Podsedkowski, L. Long-range snake-like robot powered by pneumatic McKibben muscles. *Archive Of Mechanical Engineering*. **66**, 257-267 (2019)

[24] Zhong, J., Luo, M., Liu, X., Fan, J. & Zhao, J. Frog-inspired jumping robot actuated by pneumatic muscle actuators. *Advances In Mechanical Engineering*. **10**, (2018).

[25] Tolley, M., Shepherd, R., Mosadegh, B., Galloway, K., Wehner, M., Karpelson, M., Wood, R. & Whitesides, G. A resilient, untethered soft robot. *Soft Robotics*. **1**, 213-223 (2014).

[26] Kim, H., Song, S. & Ahn, S. A turtle-like swimming robot using a smart soft composite (SSC) structure. *Smart Materials And Structures*. **22** (2013)

[27] Klein, M., Boxerbaum, A., Quinn, R., Harkins, R. & Vaidyanathan, R. SeaDog: A rugged mobile robot for surf-zone applications. *Proceedings Of The IEEE RAS And EMBS International Conference On Biomedical Robotics And Biomechatronics*. (2012)

[28] Rus, D. & Tolley, M. Design, fabrication and control of soft robot using fluidic elastomer actuators. *Nature*. **521** (2015)

[29] Godon, S., Kruusmaa, M., & Ristolainen, A. Maneuvering on non-Newtonian fluidic terrain: a survey of animal and bio-inspired robot locomotion techniques on soft yielding grounds. *Frontiers in Robotics and AI*. **10** (2023).

[30] Wang, T., Ma, P., Spielberg, A. E., Xian, Z., Zhang, H., Tenenbaum, J. B., Rus, D., & Gan, C. Softzoo: A soft robot co-design benchmark for locomotion in diverse environments. *arXiv preprint arXiv:2303.09555* (2023).

[31] Wong, J. Y. Theory of Ground Vehicles. Wiley, 2008. `https://books.google.ca/books?id=Blp2D1DteTYC`.

[32] An, N., Li, M., & Zhou, J. Modeling and understanding locomotion of pneumatic soft robots. *Soft Materials*, **16**(3), 151–159 (2018).